THE EFFECT OF PULSED IRRADIATION ON THE SWELLING OF 316 STAINLESS STEEL IN FUSION REACTORS

N.M. GHONIEM

School of Engineering and Applied Science, University of California, Los Angeles, CA 90024, USA

and

G.L. KULCINSKI

Nuclear Engineering Department, University of Wisconsin, Madison, WI 53706, USA

A time-dependent rate theory formulation has been used to study the effects of pulsed irradiation on point defect and void behavior at elevated temperatures. It is found that point defects in pulsed tokamaks, θ-pinchs and inertial confinement fusion reactors (ICFR) display non-steady-state behavior. The pulsed nature of the irradiation has been shown to produce considerable deviations from steady-state void growth behavior at high temperatures ($0.3\ T_m$ to $0.5\ T_m$). In particular, the amount of swelling in the first-wall can be reduced for ICFR pulsing conditions and pulse widths ranging from a nanosecond to a microsecond. The amount of reduction increases with increased pellet yield at a fixed operating temperature, geometry and ICFR plant power output.

1. Introduction

In the past ten years investigators have been directing increasing efforts towards the understanding of the relationships between microstructural behavior and mechanical responses of metals during irradiation. The fundamental motive for such studies has been the increasing dependence on nuclear reactors for energy production. The use of large material testing reactors as well as experimental simulation techniques (i.e., particle accelerators and high voltage electron microscopes) has helped to supply the experimental data for both reactor design and theory development. However, there is a complete absence of fusion materials testing reactors at the present time, and the need for experimental and mathematical simulation techniques is readily apparent. The planning of a well-defined strategy for both theoretical developments and fundamental experiments is vital to achieve a greater understanding of materials responses to different irradiation environments.

The major problem facing materials scientists is how to model the pulsed nature of all the fusion reactor concepts (except for the mirror approach) proposed so far [1–3]. The production of defects, followed by periods of high temperature annealing when no defects are produced, is in marked contrast to the "steady-state" damage produced in fission reactors. Therefore, in this paper we will investigate the effect of pulse time, intensity, and frequency on the final disposition of the fundamental defects produced (i.e. vacancies and interstitials) and in particular we will investigate the effect of pulsing on void growth in metals. While the approach developed in this paper is general in nature, we will tend to concentrate on the situation in inertially confined fusion reactor (ICFR) concepts as an illustration of the effects to be expected.

2. Theory and computational aspects

The microstructural changes during irradiation are primarily controlled by the temporal variations in point defect concentrations. When the irradiation source is a strong function of time, point defect concentrations can exhibit considerable time variations [4]. While it has been a reasonable assumption to consider that point defects in metals reach a quasi-steady-state concentration during time-independent irradiations, a dynamic treatment is necessary during

transient and pulsed operations. Such a fully dynamic rate theory (FDRT) has been developed to study microstructural changes in transients and during pulsed irradiation [5,6]. Here, we give only the highlights of the theory and the associated computational aspects of the FDRT. The time-dependent point-defect concentrations are given by the rate equations:

$$dC_I(t)/dt = P(t) - \lambda_I(m, t)\, C_I(t) - \alpha C_I(t)\, C_v(t)\,, \quad (1)$$

$$dC_v(t)/dt = P^e(m, t) + (1 - \epsilon)\, P(t) - \lambda_v(m, t)\, C_v(t)$$
$$- \alpha C_I(t)\, C_v(t)\,, \quad (2)$$

where the different variables in eqs. (1) and (2) are defined as follows:

$C_I(t)$ — interstitial concentration (at/at);

$C_v(t)$ — vacancy concentration (at/at);

$P(t)$ — time-dependent point-defect production rate (at/at/s);

ϵ — is the fraction of vacancies produced directly into vacancy loops;

$\lambda_I(m, t)$ — a microstructural (m) and time (t)-dependent interstitial time constant (s^{-1});

$\lambda_v(m, t)$ — a microstructiral and time-dependent vacancy time constant (s^{-1});

α — is point-defect mutual recombination coefficient (s^{-1});

$P^e(m, t)$ — a microstructural and time dependent vacancy emission rate (at/at s).

Eqs. (1) and (2), together with other rate equations for the average void radius, average interstitial loop radius, vacancy concentration in vacancy loops and vacancy loop number density, form a set of stiff first-order non-linear differential equations. This system has been solved numerically using the implicit multistep methods developed by Gear for stiff systems [7]. Special attention was directed towards the stability of the solution in pulsed systems. A variety of cases simulating different combinations of material and irradiation conditions have been included in the computer code TRANSWELL [8].

3. Examples of point defect behavior in fusion reactors

3.1. Tokamak fusion reactors

Tokamak fusion reactors are designed to have long confinement times and relatively shorter times
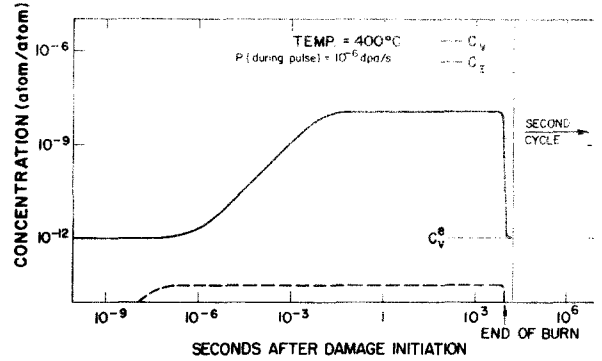

Fig. 1. Point defect concentrations in 316 SS in a tokamak fusion reactor at 400°C.

between burns to achieve maximum plant efficiency. Burn cycles with durations in the range of (30—90) min and cooling cycles of about (5—10) min are considered in the early design of these devices [2]. Recent advances in the conceptual designs consider burn cycle duration of only a few minutes with down times in the tenths of seconds [9]. As an illustrative example of a tokamak reactor, we will consider a burn cycle of 10^4 s and a cooling cycle of 400 s to study point defect behavior.

Calculations were performed to examine the time characteristics of point defects in a 316 SS first-wall using the materials properties proposed by Bullough et al. [10], and the above Tokamak operating cycle. Fig. 1 shows the vacancy and interstitial concentrations, at 400°C, in the stainless steel first-wall where the average rate of point defect production is 10^{-6} dpa/s (which corresponds to few MW/m^2 wall loading). It is seen that in the first few tenths of a microsecond, interstitials reach an equilibrium concentration with the sink structure present at this temperature, while the vacancy concentration remains constant at the thermal equilibrium value. The interstitial concentration remains constant at a value of $\approx 3 \times 10^{-14}$ at/at during the irradiation as a result of an equilibrium between a constant production rate and a steady absorption rate by sinks in the matrix. [The microstructure does not change appreciably during the burn cycle, because of the small dose achieved (10^{-2} dpa) per cycle.] On the other hand, the lower mobility of vacancies at this temperature causes the vacancy population (after a microsecond of irradiation) to increase linearly from its thermal equilibrium
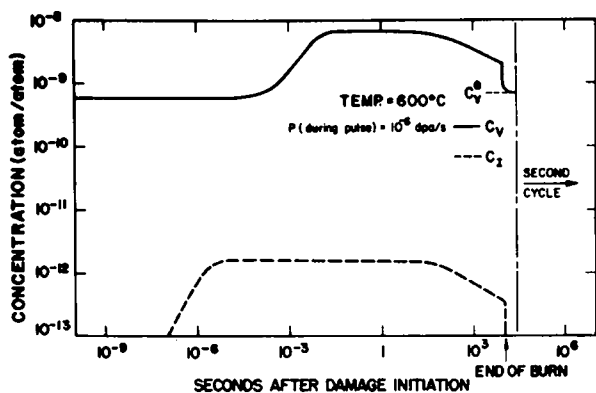
Fig. 2. Point-defect concentrations in 316 SS in a tokamak fusion reactor at 600°C.

Fig. 3. Point defect concentrations in 316 SS in a theta-pinch fusion reactor at 400°C.

($\approx 10^{-12}$ at/at) to its irradiation equilibrium value ($\approx 10^{-8}$ at/at). At approximately a vacancy mean life-time (≈ 2 ms for this material), vacancies can reach various sinks and are removed from the matrix producing the state of equilibrium between production and sink removal. The initial point-defect recombination rate is not significant because of the high sink density at low temperatures ($\approx 10^{12}$ cm^{-2}).

At higher temperatures, other factors influence point defect dynamics. Fig. 2 shows point-defect concentrations, at 600°C, as function of irradiation time during one burn cycle. Because of the lower sink densities at higher temperatures, point defects experience lower sink removal rates, generally causing higher defect concentrations. The interstitial mean lifetime increases by two orders of magnitude (to about 4 μs) at 600°C because of the decrease in the sink density at higher temperatures. Therefore, interstitials achieve complete equilibrium with the sinks after about 10 microseconds and their concentration reaches the value of 1.8×10^{-12} at/at.

The changes in the vacancy concentration take a relatively longer time (≈ 1 ms) because of the higher thermal equilibrium vacancy concentration at 600°C (6×10^{-10} at/at). The vacancy concentration eventually reaches the value of 7×10^{-9} at/at within a few milliseconds after the burn starts.

At 600°C, the build-up of the microstructure with a corresponding increase in sink strength accounts for the drop in C_V and C_I after about 100 s. At the end of the burn cycle point-defect concentrations
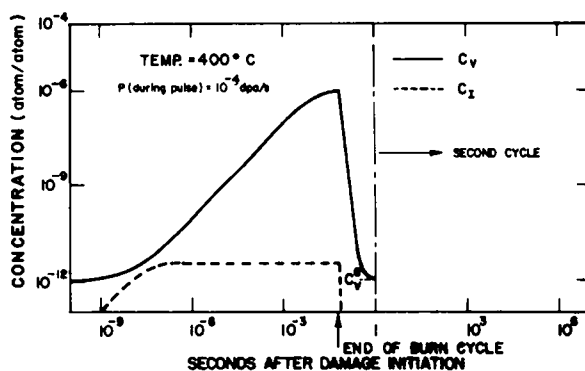
drop to their thermal equilibrium values with characteristic time constants which are much shorter than the cooling cycle duration (400 s) for both vacancies and interstitials.

3.2. Theta pinch fusion reactors

The time structure of neutron production in theta-pinch fusion reactors [11] is much different than for tokamaks. In general the neutrons are produced in a relatively short time, while it takes much longer to re-establish the proper plasma conditions. A pulse duration of 0.1 s and pulse period of 1 s was assumed in this study. Figs. 3 and 4 show the time behavior of point defects in a theta pinch fusion first-wall. A point-defect generation rate of 10^{-4} dpa/s was
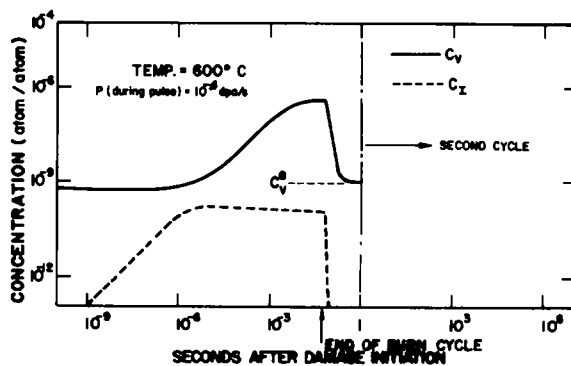

Fig. 4. Point defect concentrations in 316 SS in a theta-pinch fusion reactor at 600°C.

assumed during the burn cycle, and no defects were produced during the cooling cycle.

At 400°C, as shown in fig. 3, interstitials quickly reach an equilibrium with sinks and achieve a concentration of 3×10^{-12}. On the other hand, vacancies do not reach an equilibrium value during the pulse, and their concentration rises to as much as 10^{-6} at/at at the end of the burn cycle. Point-defect concentrations in this case are about two orders of magnitude higher than the corresponding tokamak reactor case because of the higher dpa rate.

Fig. 4 shows point-defect concentrations, as a function of time, at 600°C. The peak vacancy concentration is slightly lower than the 400°C case because of the higher vacancy mobility. Although the interstitial concentration is higher at 600°C than at 400°C ($\approx 10^{-10}$ at/at), it starts to slowly drop with time because of mutual point-defect recombination as the vacancy concentration builds up. At the end of the burn cycle, point-defect concentrations rapidly return to their thermal equilibrium values with greatly different time constants (about 4 μs for an interstitial and 15 ms for a vacancy). It is obvious from the previous analysis that point-defect time behavior is far from steady-state equilibrium, encountered in present fission reactor irradiations.

3.3. Inertially confined fusion reactors (ICFR's)

The category of pulsed fusion reactors includes the laser driven thermonuclear reactors, electron beam and ion-beam-driven thermonuclear reactors. These types of reactors differ in basic operational methods, and there is a wide variety of design concepts which try to mitigate some of the related technological problems. In the following, we describe, in a generic sense, the time frames for the damage analysis related to ICFR's. Once the point-defect behavior in currently envisioned ICFR first-walls is explained, we will then use this information to discuss the general effect of such point-defect variations later in this paper.

The spectra of neutrons from microexplosions, pulsing frequency rates and damage rates can vary considerably depending on the specific reactor design [12]. The particular geometrical and compositional structure of the DT pellet exploded in the center of the cavity will affect the instantaneous neutron flux and energy, as well as the energy spectrum of the pellet debris (i.e. unburnt fuel, tamper and ablator materials). We will only focus our attention in the rest of this paper on the neutron damage even though it has been shown that in the near surface region of an

Table 1
Summary of pulse width and damage rate considerations for a 1000 MW$_t$ reactor

Case	Time between pulses (s)	Pellet yield (MJ)	Pulse width (s)	dpa/shot at 7 m.	Av. dose rate in pulse (dpa/s)
1	10	10 000	10^{-9}	10^{-5}	10 000
			10^{-8}		1 000
			10^{-7}		100
			10^{-6}		10
2	1	1 000	10^{-9}	10^{-6}	1 000
			10^{-8}		100
			10^{-7}		10
			10^{-6}		1
3	0.1	100	10^{-9}	10^{-7}	100
			10^{-8}		10
			10^{-7}		1
			10^{-6}		0.1
4	0.01	10	10^{-9}	10^{-8}	10
			10^{-8}		1
			10^{-7}		0.1
			10^{-6}		0.01

ICFR, the damage rate by the pellet debris can be much higher than that of the neutrons [13–14]. This is the same as saying that we will consider bulk damage effects.

In order to illustrate the multitude of possible pulsed damage conditions we have conducted a parametric study over a wide range of pellet yields keeping the total output of the reactor constant at 1000 MW$_t$ and the radius of the chamber constant. (In reality the radius would probably increase with increasing pellet yield but for some designs such as the "liquid Li waterfall" proposed by the LLL group [15] the radius changes might be minor with pellet yield.) A summary of the conditions considered is given in table 1.

The constant power level of 1000 MW$_t$ dictates that the time between pulses varies from 10 milliseconds for a 10 MJ per pellet yield to 10 s for a 10 000 MJ yield. Within each pellet yield-frequency of pulse combination we have allowed the neutron damage to occur over time periods ranging from 1 ns to 1 μs. This should cover reasonable pulse widths from current pellet designs which range from 10–30 ns [16]. The use of a nominal cavity radius of 7 m means that the accumulated displacement damage will vary from approximately 10^{-8} to 10^{-5} dpa per shot or a 10^{-6} dpa/s average displacement rate over time. However, to achieve this average displacement rate the instantaneous damage rate can be as large as 10 000 dpa/s for the 10 000 MJ pellet with a 1 ns time spread in the neutron arrival rate to 0.01 dpa/s for a 10 MJ pellet yield when the neutrons arrive over a 1 μs time scale. Current pellet designs of 100 MJ indicate ≈10 ns time spreading and a 10 dpa/s damage rate. Higher yield pellet designs would increase the damage rate but since there will be considerable downscattering of the neutrons in these pellets, they will arrive over longer time periods. Anticipated damage rates for a 1000 MJ pellet would be in the 50 dpa/s range.

Having set up the various time limitations on pulse width and duration it is now important to consider how these compare to the defect lifetimes. For example, a vacancy mean lifetime can vary between 10^{-4} s at high temperatures (≈0.5 T_m) and high defect sink densities to 1 second at low temperature (≈0.3 T_m) and low sink densities. On the other hand, interstitial mean lifetimes can vary between 10^{-7} s at high tem-

peratures and high sink densities to 10^{-5} s at low temperatures and low sink densities. Using the following notation: τ_i: interstitial mean lifetime in seconds, τ_v: vacancy mean lifetime in seconds, P_w: pulse width in seconds, Δt: pulse period in seconds, we find that there are four combinations of these parameters that might be important in pulsed fusion reactors.

$$(1)\; P_w < \tau_i < \tau_v \, , (2)\; \tau_i < P_w < \tau_v \, , \tag{3}$$

$$(3)\; \tau_i < \Delta t < \tau_v \, , (4)\; \tau_i < \tau_v < \Delta t \, . \tag{4}$$

We will now study the case of 1 pulse every 10 s with two different pulse widths, 1 ns and 1 μs. As an example, we will consider 316-SS as in our previous example. At low temperatures (400°C) the vacancy concentration during the pulse increases rapidly with time irrespective of pulse width as shown in fig. 5. The vacancy concentration starts to decline from the high value achieved during the pulse (≈10^{-5} at/at) to its equilibrium concentration, $\bar{C}_v$, at about 2 ms. The results in fig. 5 indicate that the pulse width, and hence the details of the damage rates inside the pulse, have no effect on the vacancy concentration after the end of the pulse as it reaches ≈10^{-5} for both cases. On the other hand, interstitial concentration increases linearly with time only for short pulses (10^{-9} s). The interstitial concentration tends to level off after about 10^{-7} s of a 10^{-6} s pulse because of the high interstitial mobility to sinks. Therefore, the interstitial concentration is dependent on the pulse width during the pulse.

At higher temperatures (600°C) the metals matrix contains less voids and dislocations, which in turn
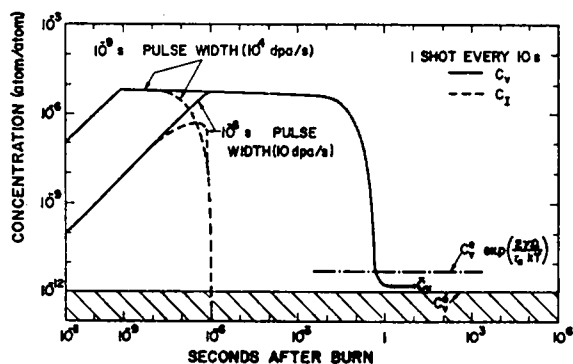

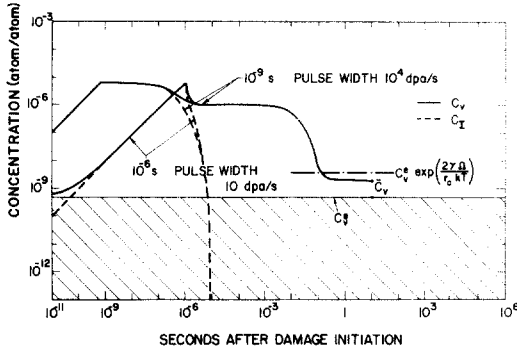Fig. 5. Point defect concentrations in 316 SS for a 10^{-6} dpa pulsed irradiation at 400°C.

Fig. 6. Point defect concentrations in 316 SS for a 10^{-6} dpa pulsed irradiation at 600°C.

allows a higher interstitial concentration. As shown in fig. 6, interstitials and vacancies exist with almost equal concentrations until the end of the pulse. This aspect enhances point defect mutual recombination and causes a considerable decrease in the vacancy concentration around $1-10\ \mu s$. It is observed from fig. 6 that there is no effect of pulse width on either point-defect behavior after about one microsecond. Finally, the vacancy mean lifetime is a little longer at the higher temperature (≈ 15 ms at 600°C) which means that the vacancy concentration does not change significantly until around 10^{-2} s.

Another important feature of fig. 6 is that the vacancy concentration in the matrix does not reach the thermal equilibrium value, C_v^e, until a long time after the irradiation is turned off. Rather, it reaches an average value, $\bar{C}_v$, determined by the existing micro-structure (voids and dislocations) and temperature. The vacancy concentration on the surface of a void of radius R_c, in the absence of stresses and gas atoms inside, is determined by the simple expression:

$$C_v = C_v^e \exp(2\gamma\Omega/R_ckT).\tag{5}$$

Due to the presence of dislocations, grain boundaries and free surfaces, the average matrix thermal vacancy concentration is smaller than the value given by expression (5). This creates a vacancy concentration gradient between the void surface and the bulk of the metal. A flow of vacancies from the void surface to the bulk of the metal is then set up, tending to reduce the void size. From fig. 5, one can notice that at low temperature (400°C) the gradient (proportional to concentration difference) between the void and the

matrix is small and the time available for void anneal-ing is short, compared to a larger gradient and longer annealing time at 600°C (fig. 6). The effects of pulsed irradiation variables on void kinetics will be explained in the next section.

4. Analysis of pulsed irradiation effects on void growth in ICFR's

Void growth during steady-state irradiation is known to be affected by many irradiation and material vari-ables [5,10]. In this section, we will concentrate on the unique features of the void growth phenomenon encountered in the case of pulsed irradiation. We will first discuss the effect of changing the pulse width while keeping the same accumulated dose in the pulse. The influence of the irradiation temperature on the growth kinetics is then discussed. Thereafter, the gen-eral features of a train of damage pulses are studied. Next, the combined influence of the repetition rate and temperature on the final swelling behavior of a 50 Å radius void will be analyzed. This is followed by a discussion of the effect different size voids (10 Å radius and 100 Å radius) can have on the final swell-ing. Finally, the consequence of changing the bias factor on pulsed irradiation is studied.,

4.1. Pulse width

We examine here two widely differing cases of neutron pulses; one of a nanosecond pulse width and the other of a microsecond pulse width. A total accu-mulated dose of 10^{-5} dpa was assumed to be the same for the two pulses so that dose rates of 10^4 dpa/s and 10 dpa/s are achieved for the nanosecond and the mi-crosecond pulses, respectively. The void growth char-acteristics of a 20 Å radius void, in 316-SS at a tem-perature of 600°C, are shown in fig. 7. The magni-tude of the maximum decrease in the void volume due to the irradiation pulse reflects the efficiency of point defect mutual recombination. If the point-defect mutual recombination rate is high during the pulse, the number of point defects free to migrate to sinks is reduced. For example, the displacement rate of 10^4 dpa/s in the nanosecond pulse is accompanied by more recombination than in the case of the 10 dpa/s displacement rate of the microsecond pulse. This
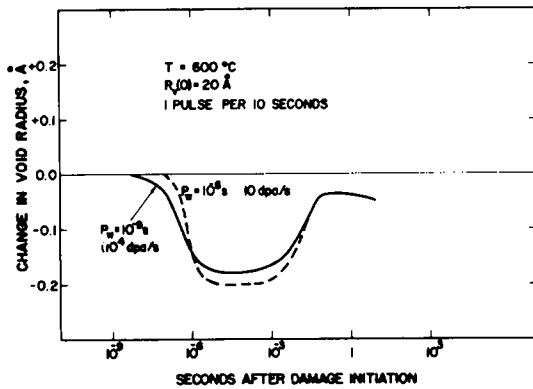
Fig. 7. Effect of pulse width on void kinetics at 600°C.

causes a smaller maximum decrease in the void radius for the nanosecond pulse as shown in fig. 7. It is found that no matter how many interstitials are added to the void, enough vacancies will eventually arrive to the void surface to partially offset the decrease in size caused by interstitials. After about a mean vacancy lifetime the void kinetics are entirely dominated by the annealing. One can conclude that in the presently considered ICFR's (with $P_w = 10^{-8}$ to 10^{-7} s), the pulse width and time structure of the displacement rate inside the pulse are not of significant importance to the overall swelling. Therefore, the accumulated dose in one pulse is the major parameter needed, as far as the damage process is considered.

4.2. Temperature

Irradiation temperature mainly affects the sink densities, point-defect mobilities and the annealing kinetics of voids. The effect of temperature on a 20 Å radius void in 316-SS subjected to one irradiation pulse of a nanosecond width and a dose rate of 10^4 dpa/s is studied in figs. 8 and 9. At 400°C the loop and void densities are high, thus the number of point defects going to the 20 Å radius void are reduced and the maximum drop in the void radius due to the interstitial flux is only ≈ -0.012 Å. When the vacancies reach the void at around a vacancy mean lifetime, they cause a net increase in the void radius. Since annealing is not strong at 400°C, this net increase in the void radius (growth) is maintained at the end of the pulse period which is 10 seconds. As the irradiation
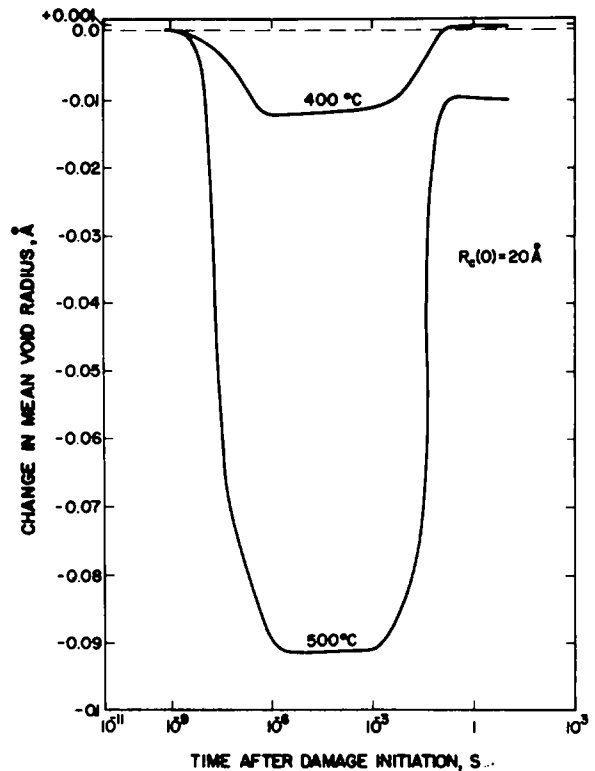

Fig. 8. Effect of pulsed irradiation temperature on void kinetics in 316 SS (low temperature).

temperature increases, the initial drop in the void radius also increases due to the larger interstitial flux. The reason for this large drop in the void radius is the lower sink density. The driving force for the annealing of the void is very sensitive to the temperature, as can be seen from fig. 9. Void annealing is very rapid at 700°C and the initial radius of 20 Å becomes 19 Å in about six seconds after the damage process begins.

4.3. A train of neutron pulses

Certain results can not be completely revealed by the study of metals response to one pulse of irradiation; the ultimate behavior of voids due to a train of pulses must be considered. The effect of a train of neutron pulses (10^{-7} dpa each) on the dimensions of a mean void of 20 Å radius at 400 °C in 316-SS is shown in fig. 10. The corresponding point-defect concentrations as a function of time, are displayed in fig. 11 (notice the linear time scales). As can be seen from
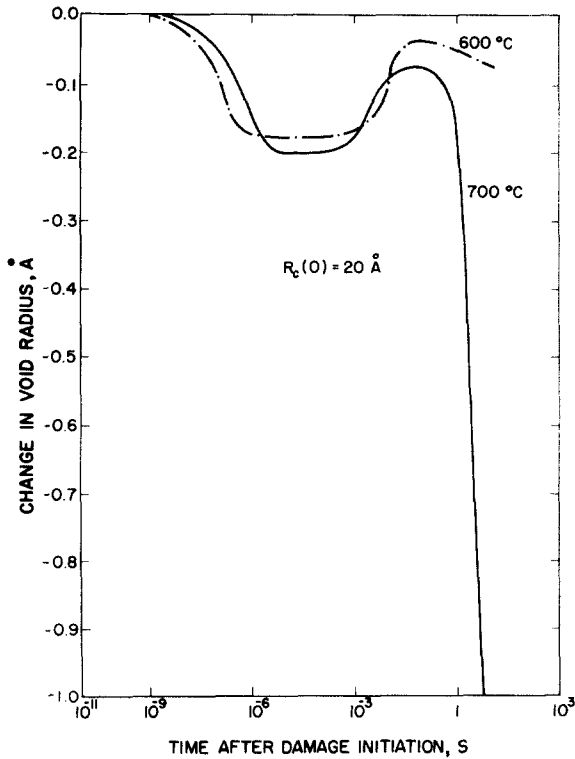
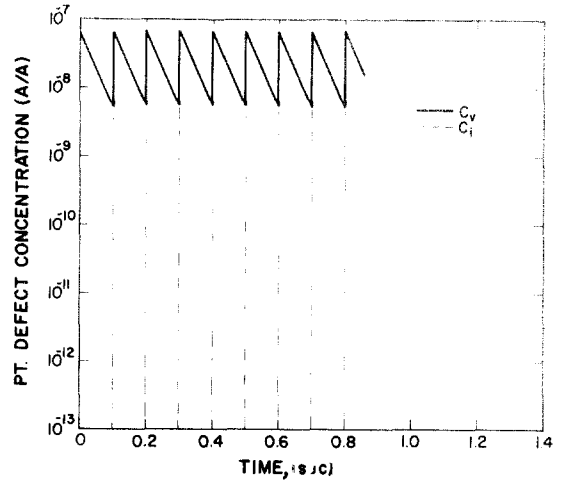Fig. 9. Effect of pulsed irradiation temperature on void kinetics in 316 SS (high temperature).

Fig. 11. Effect of a train of neutron pulses (10 dpa each) on point defect concentrations at 400°C in 316 SS.

Fig. 10. Effect of a train of neutron pulses on the kinetics of a mean void of 20 A radius at 400°C in 316 SS.

fig. 11, the interstitial concentration drops to its thermal equilibrium value, almost instantly after the pulse. This initially causes a rapid drop in the void radius, about -1.5×10^{-4} Å in this case. On the other hand, the vacancy concentration slowly declines, trying to reach its thermal equilibrium value ($\approx 10^{-12}$ at/at at 400°C). The relatively short pulse period in this case keeps the vacancy concentration within certain bounds (between 6×10^{-9} at/at and 9×10^{-8} at/at). It can be seen that there is a slight increase in the overall concentration, due to accumulation from previous pulses. Although any given void shrinks in the first few pulses as shown in fig. 10, it will eventually regain its initial radius and ultimately grow due to the increasing vacancy concentration. It is then concluded that to compare the results of void growth rates under different pulsing conditions, the calculations should be carried out over several cycles at least until the transient point-defect behavior is replaced by more "steady-state" values.

4.4. The simultaneous effects of temperature and pulse repetition rate

One of the more important design aspects of any fusion reactor is the need to prohibit swelling in structural materials. The combination of certain design parameters that can achieve this goal, namely irradiation temperature and pulse repetition rate, is studied
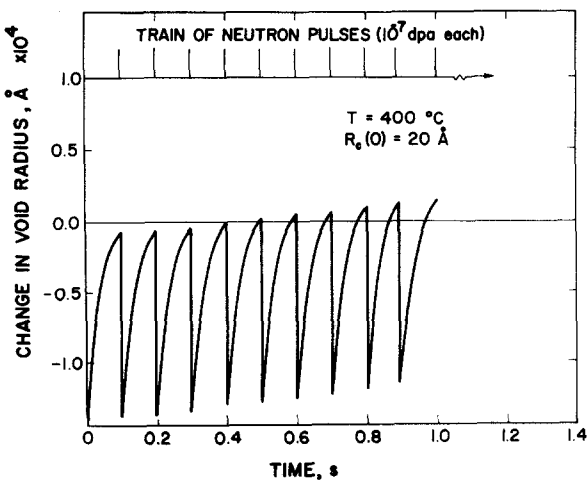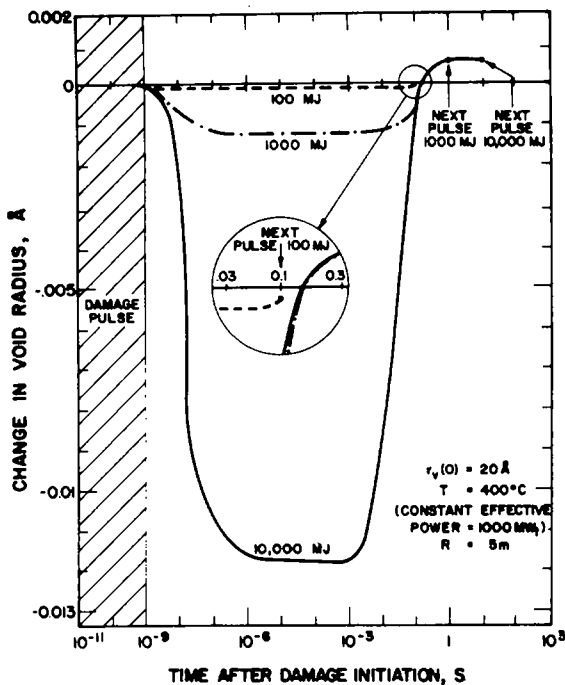
Fig. 12. Pellet yield effect on void growth in 316 SS at 400°C.

atures, as a function of the pulse repetition rate.

The behavior of a 20 Å radius void at 400°C is shown in fig. 12, as a function of pellet yield. The total damage is also taken into account and it, of course, varies proportionally to the size of the pellet yield. In the 10 000 MJ case, the damage created by the pulse is very large causing the void radius to initially decrease by ≈0.012 Å, while the radius decrease caused by the 1000 MJ pellet is only ≈0.0012 Å, and that resulting from the 100 MJ pellet is ≈0.00012 Å as shown in fig. 12. However, the final swelling caused by the 10 000 and 1000 MJ pulses is positive at 400°C. Since the pulse period for the 10 000 MJ pellet is ≈5000τ_v, the void will continue to grow over the next successive pulses, due to the fact that vacancies will accumulate from previous pulses. In order to find out the equivalent effect of the 1000 MJ pellet system, one has to study at least 10 pulses, and for the 100 MJ pellet system a 100 pulses.

A study of the change in a 50 Å radius void in 316-SS after an accumulated dose of 10^{-5} dpa was conducted and the results are shown in figs. 13 and 14. It is assumed that $Z_i = 1.08$, $\epsilon = 0$, and $P_w = 10^{-6}$ s and no gas is generated. The results of the calculations, with the previously described assumptions, are shown in table 2. Calculations for 1, 10, 100 and 1000 pulses were carried out, and also steady-state results for an equivalent system (10^{-6} dpa/s dose rate) were performed for comparison. It can be observed from table

in this section. First, we will study the behavior of a void in a 316-SS first-wall of similar power output systems (1000 MW$_t$ as in table 1). This will be followed by a study of void growth at different temper-

Table 2
Pulsed irradiation void radius changes (A) after 10 s of irradiation in 316 SS [a]

No. of pulses studied	1	10	100	1000	10^7 (steady-state)
Dose rate in pulse (dpa/s)	10	1	0.1	0.01	10^{-6}
Period (s)	10	1	0.1	0.01	10^{-6}
Pulse rate (s^{-1})	0.1	1	10	100	10^6
Growth after 10 s (A)					
$T = 400°C$	$+2.2 \times 10^{-5}$	$+2.2 \times 10^{-5}$	$+2.2 \times 10^{-5}$	$+2.2 \times 10^{-5}$ [b]	$+2.2 \times 10^{-5}$
$T = 450°C$	$+1.8 \times 10^{-4}$	$+1.9 \times 10^{-4}$	$+1.9 \times 10^{-4}$	$+1.9 \times 10^{-4}$ [b]	$+1.9 \times 10^{-4}$
$T = 500°C$	$+7.5 \times 10^{-4}$	$+1.04 \times 10^{-3}$	$+1.1 \times 10^{-3}$	$+1.1 \times 10^{-3}$	$+1.1 \times 10^{-3}$
$T = 550°C$	$+6.0 \times 10^{-4}$	$+2.7 \times 10^{-3}$	$+3.7 \times 10^{-3}$	$+3.8 \times 10^{-3}$ [b]	$+3.8 \times 10^{-3}$
$T = 600°C$	-7.0×10^{-3}	-2.2×10^{-3}	$+3.5 \times 10^{-3}$	$+4.8 \times 10^{-3}$	$+4.8 \times 10^{-3}$
$T = 650°C$	-0.053	-0.046	-0.032	-0.029 [b]	-0.025
$T = 700°C$	-0.27	-0.26	-0.23	-0.23 [b]	-0.22

[a] $R_c(0) = 50$ A, $P_w = 10^{-6}$ s, $Z_i = 1.08$, $\epsilon = 0$, av. dose rate = 10^{-6} dpa/s.
[b] Values extrapolated from the results of 100 pulses.
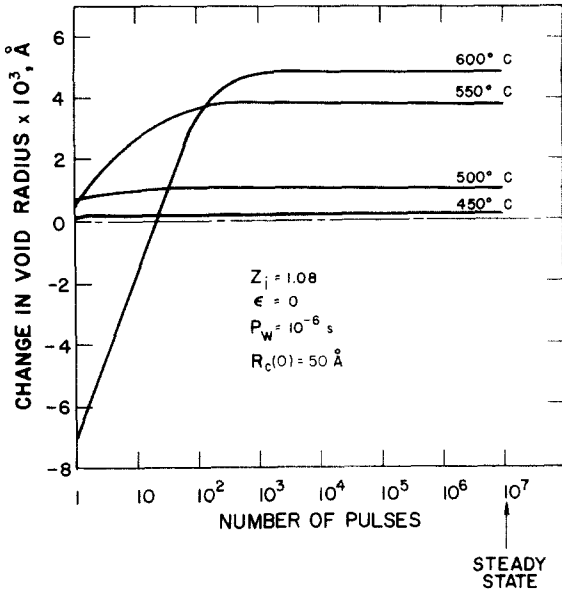
Fig. 13. Change in void radius in 316 SS after an accumulated dose of 10^{-5} dpa (low temperature).

Fig. 15. Effect of pulsed irradiation on void growth in 316 SS for 10^{-6} dpa/s average.

2 and figs. 13 and 14 that at low temperatures (400–450°C) void growth in all pulsed systems behaves the same as the corresponding steady-state case. This behavior occurs because void growth is controlled by the total bias of the system with little effects of
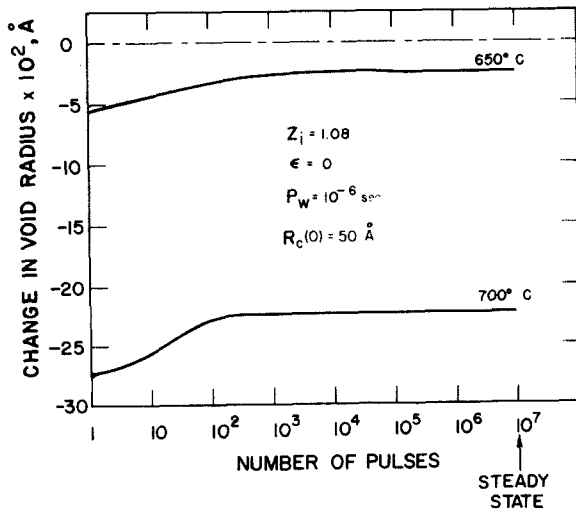

Fig. 14. Change in void radius in 316 SS after an accumulated dose of 10^{-5} dpa (high temperature).
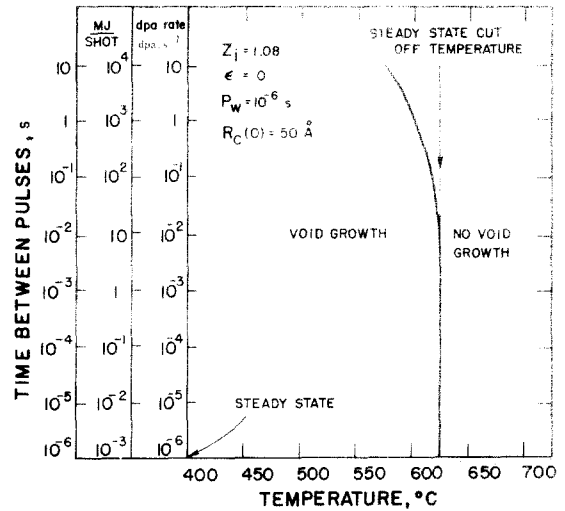
annealing on voids in between successive pulses. On the other hand, at higher temperatures the phenomenon of interpulse annealing is more prominent. For example, at 600°C, the 50 Å radius void has a net *decrease* in radius of 7×10^{-3} Å at the end of one pulse followed by a 10 s annealing period. However, the void experiences a net *increase* in radius of +3.5 × 10^{-3} after 100 pulses of 0.1 s period each. Steady-state-like void growth conditions are achieved if the repetition rate is 100 pulses per second or greater (for temperatures above about 500°C), as can be seen from figs. 13 and 14. These important conclusions are summarized in fig. 15, where the boundary between void growth and no growth conditions is given as a function of pulsing variables. In steady-state irradiation, this temperature is about 625°C for stainless steel at a dose rate of 10^{-6} dpa/s. The other extreme, is that of a 10 s pulse period which has a cut off high temperature limit of only 575°C.

4.5. The effect of the initial void radius

Void annealing and growth kinetics are strong functions of the initial void radius. With the irradiation conditions of the previous section, the same series of calculations were performed for two different void radii; a small initial void radius of 10 Å, and a large initial void radius of 100 Å. Figs. 16 and 17
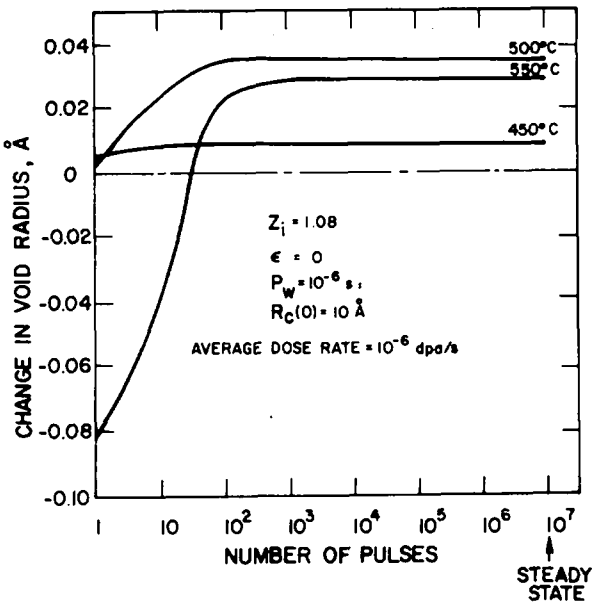
Fig. 16. Change in void radius in 316 SS after an accumulated dose of 10^{-5} dpa for a 10 A initial radius (low temperature).
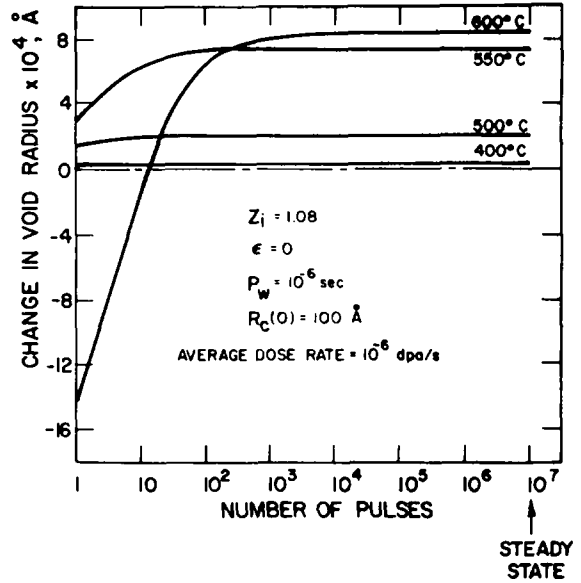

Fig. 18. Change in void radius in 316 SS after an accumulated dose of 10^{-5} dpa for a 100 A initial radius (low temperature).
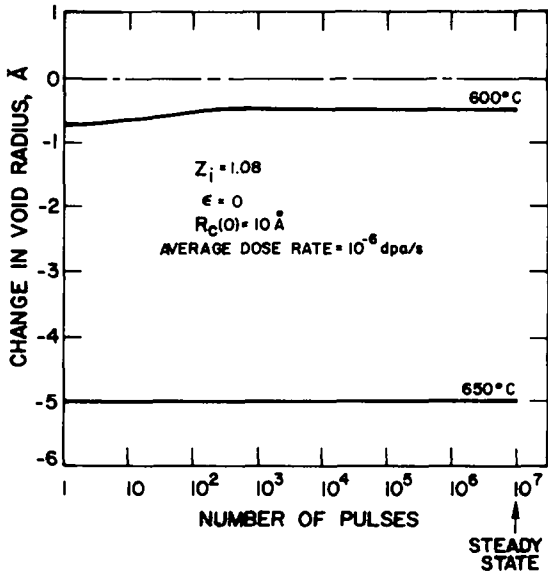

Fig. 17. Change in void radius in 316 SS after an accumulated dose of 10^{-5} dpa for a 10 A initial radius (high temperature).

demonstrate the void growth behavior for the 10 Å radius, as a function of pulse rate, while table 3 shows the changes in the void radius after 10 seconds of irradiation in different equivalent pulsed systems. For this small void radius, it is observed that annealing effects are very pronounced. For a 10 s time period between pulses at 550°C, the void radius decreases by —0.082 Å, while for 0.1 s between pulses at the same temperature the radius increases by +0.022 Å. However, at high temperatures (650°C), void annealing becomes very dominant for all pulse rates and the 10 Å radius void quickly shrinks down to a radius of 5 Å, which is the radius for the equilibrium bubble containing the number of gas atoms required to initiate the void.

Increasing the void radius affects both the annealing and growth phases of the void kinetic behavior. The 100 Å radius void does not experience as much shrinkage (negative change in radius) at 550°C (see table 4 and figs. 18 and 19, as the 10 Å radius void showed at the same temperature, fig. 16). The relative effect of the initial void radius on the high temperature cut-off for growth is summarized in fig. 20. The figure also reflects the fact that the initial void radius has to be large, if void growth is expected at such temperatures.

Table 3
Pulsed irradiation void radius changes (A) after 10 s of irradiation in 316 SS [a]

No. of pulses studied	1	10	100	10^{-7} (steady-state)
Dose rate in pulse (dpa/s)	10	1	0.1	10^{-6}
Period (s)	10	1	0.1	10^{-6}
Pulse rate (s^{-1})	0.1	1	10	10^{6}
	Growth after 10 s (A)			
$T = 400°C$	$+4.1 \times 10^{-4}$	$+4.2 \times 10^{-4}$	$+4.2 \times 10^{-4}$	$+4.2 \times 10^{-4}$
$T = 450°C$	$+0.0050$	$+0.0082$	$+0.0085$	$+0.0086$
$T = 500°C$	$+0.0016$	$+0.022$	$+0.036$	$+0.035$
$T = 550°C$	-0.082	-0.040	$+0.022$	$+0.029$
$T = 600°C$	-0.740	-0.680	-0.540	-0.50
$T = 650°C$	-5.00 [b]	-5.00 [b]	-5.00 [b]	-5.00 [b]
$T = 700°C$	-5.00 [b]	-5.00 [b]	-5.00 [b]	-5.00 [b]

[a] $R_c(0) = 10$ A, $P_w = 10^{-6}$ s, $Z_i = 1.08$, $\epsilon = 0$, av. dose are t = 10^{-6} dpa/s.
[b] This value corresponds to the bubble equilibrium radius, assumed to be 5 A.

Table 4
Pulsed irradiation void radius changes (A), after 10 s of irradiation in 316 SS [a]

No. of pulses studied	1	10	100	10^{7} (steady-state)
Dose rate in pulse (dpa/s)	10	1	0.1	10^{-6}
Period (s)	10	1	0.1	10^{-6}
Pulse rate (s^{-1})	0.1	1	10	10^{6}
	Growth after 10 s (A)			
$T = 400°C$	$+3.9 \times 10^{-6}$	$+3.9 \times 10^{-6}$	$+3.9 \times 10^{-6}$	$+3.9 \times 10^{-6}$
$T = 450°C$	$+3.4 \times 10^{-5}$	$+3.5 \times 10^{-5}$	$+3.5 \times 10^{-5}$	$+3.5 \times 10^{-5}$
$T = 500°C$	$+1.7 \times 10^{-4}$	$+2.0 \times 10^{-4}$	$+2.0 \times 10^{-4}$	$+2.0 \times 10^{-4}$
$T = 550°C$	$+2.9 \times 10^{-4}$	$+6.4 \times 10^{-4}$	$+7.3 \times 10^{-4}$	$+7.3 \times 10^{-4}$
$T = 600°C$	-1.5×10^{-3}	-1.8×10^{-4}	$+6.8 \times 10^{-3}$	$+8.2 \times 10^{-4}$
$T = 650°C$	-1.4×10^{-2}	-1.1×10^{-2}	-8.1×10^{-3}	-7.0×10^{-3}
$T = 700°C$	-6.8×10^{-2}	-6.5×10^{-2}	-5.9×10^{-2}	-5.6×10^{-2}

[a] $R_c(0) = 100$ A, $P_w = 10^{-6}$ s, $Z_i = 1.08$, $\epsilon = 0$, av. dose rate = 10^{-6} dpa/s.

Table 5
Pulsed irradiation void radius changes (A), after 10 s of irradiation in 316 SS [a]

No. of pulses studied	1	10	100	10^{7} (steady-state)
Dose rate in pulse (dpa/s)	10	1	0.1	10^{-6}
Period (s)	10	1	0.1	10^{-6}
Pulse rate (s^{-1})	0.1	1	10	10^{6}
	Growth after 10 s (A)			
$T = 400°C$	$+6.96 \times 10^{-6}$	$+7.02 \times 10^{-6}$	$+7.03 \times 10^{-6}$	$+6.97 \times 10^{-6}$
$T = 450°C$	$+5.37 \times 10^{-5}$	$+5.75 \times 10^{-5}$	$+5.80 \times 10^{-5}$	$+5.7 \times 10^{-5}$
$T = 500°C$	$+1.59 \times 10^{-4}$	$+2.58 \times 10^{-4}$	$+2.79 \times 10^{-4}$	$+2.71 \times 10^{-4}$
$T = 550°C$	-6.94×10^{-4}	-2.02×10^{-4}	$+3.19 \times 10^{-4}$	$+3.1 \times 10^{-4}$
$T = 600°C$	-8.9×10^{-3}	-7.37×10^{-3}	-5.52×10^{-3}	-5.27×10^{-3}
$T = 650°C$	-5.44×10^{-2}	-5.21×10^{-2}	-4.77×10^{-2}	-4.6×10^{-2}
$T = 700°C$	-0.267	-0.264	-0.257	-0.253

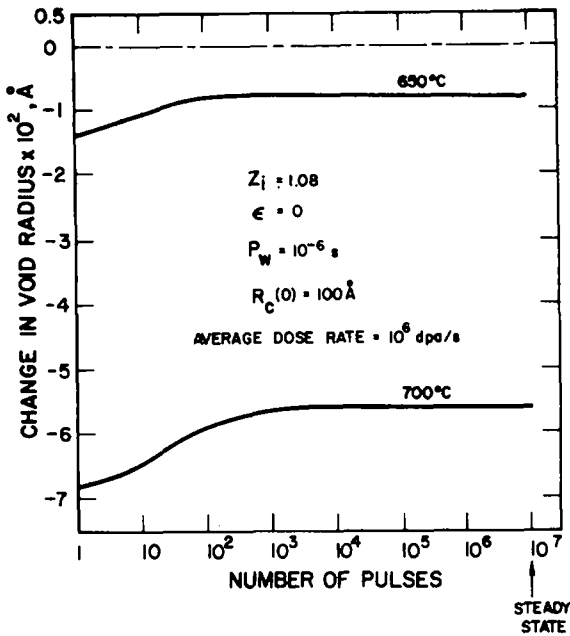[a] $R_c(0) = 50$ A, $P_w = 10^{-6}$ s, $Z_i = 1.025$, $\epsilon = 0$, av. dose rate = 10^{-6} dpa/s.

Fig. 19. Change in void radius in 316 SS after an accumulated dose of 10^{-5} dpa for a 100 A initial radius (high temperature).
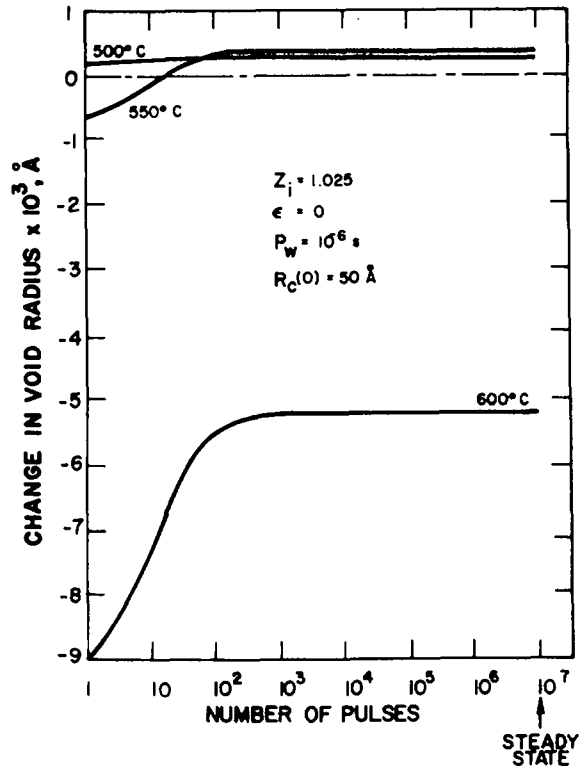
4.6. The effect of the bias factor (Z_i)

From the previous studies [5] on the growth behavior of voids, it can be seen that the high tem-

Fig. 20. Initial void radius effects in the void growth—no growth temperature.

Fig. 21. Change in void radius in 316 SS after an accumulated dose of 10^{-5} dpa for $Z_i = 1.025$ and 50 A initial radius.

perature cut-off for void growth is determined by a balance between the void growth aspect, caused by the net bias of the system, and its tendency to shrink, due to the annealing effects. In the following, we study the effect of changing the dislocation-interstitial bias factor on the growth kinetics.

The same example for the 50 Å radius void is studied here, with all the previous conditions, except for using a different bias factor $Z_i = 1.025$. The results of the calculations for pulsed irradiation void radial changes in different pulsed systems are shown in table 5 and fig. 21. A comparison between the growth behavior of a 50 Å radius void with $Z_i = 1.08$ and that of the same void with $Z_i = 1.025$ reveals that in the latter case, the change in the radius as a function of the number of pulses switches from negative to positive at 550°C, while the similar behavior in the $Z_i = 1.08$ case changes sign at 600°C (fig. 13). The steady-state cut-off temperature is $\approx 575°C$ for $Z_i = 1.025$. This indicates that the smaller the bias
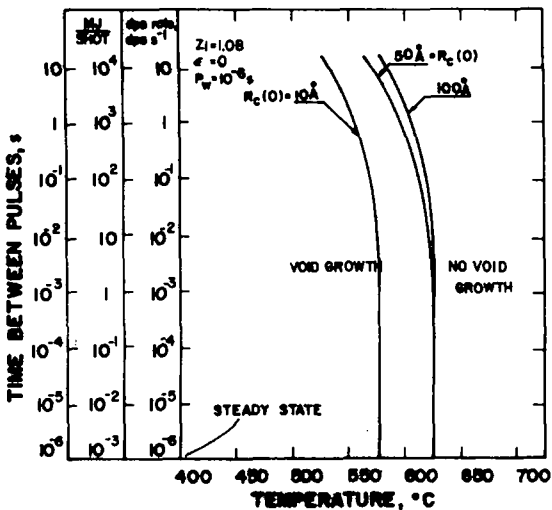
factor, the lower the high temperature void growth cut-off value, because of the greater influence of interpulse void annealing.

5. Concluding remarks

In this paper the growth of the voids has been studied under a wide variety of pulsed irradiation conditions. It has been found that pulsed irradiation produces a different point-defect behavior which cannot be adequately described by an inherently steady-state theory. The following major points have also been made.

1. Steady-state response of metals is not always achieved for pulsed systems. Even for systems with long burn cycles, (i.e. tokamaks) point-defect concentrations, at the start and sometimes at the end of the cycle, are different from their steady-state values.

2. Annealing of voids in metals is not only a function of the annealing temperature, but also a function of the microstructure present.

3. For ICFR pulsing conditions and pulse widths ranging from a nanosecond to a microsecond, the time structure of the dose rate during the pulse is not significant in the determination of the final swelling of first-wall materials. The integrated dose within the irradiation pulse is the important damage parameter.

4. The void growth behavior for the first few pulses in ICFR's is not necessarily an indication of the final metal swelling behavior. The void growth behavior has to be studied over a time span of about 1000–5000 τ_v, to determine the ultimate void growth characteristics.

5. Under pulsed irradiation, void growth behavior is a strong function of both the pulse repetition rate and the irradiation temperature. Voids in stainless steel were shown to exhibit slower growth rates at high temperatures when there are long times between successive pulses. The dividing temperature between growth and no growth of voids can be reduced by as much as 50°C from the corresponding steady-state value, if the time between the pulses is as long as ten seconds.

6. Pulsed irradiation has been shown to be equivalent to steady-state irradiation, for an average dose rate of 10^{-6} dpa/s in stainless steel, if the pulse repetition rate is greater than 500 pulses per second.

7. It has been found that smaller void radii and lower interstitial dislocation bias factors tend to accelerate interpulse annealing. This causes a lower net growth and further reduces the temperature between growth and no growth.

8. For a fixed operating temperature, geometry and ICFR plant power output, the amount of swelling in the first-wall can be reduced by using higher yield pellets. This results from higher mutual point-defect recombination rates and also because the annealing time between microexplosions of large yield pellets is longer.

9. For a fixed geometry, ICFR power plant output and pellet yield, the amount of swelling in the first-wall can be reduced by operating at the highest temperatures allowed by other design factors (e.g. embrittlement).

Acknowledgements

References

[1] Proc. 2nd Topical Meeting on Technology of Controlled Nuclear Fusion, Richland, WA (1976), Conf. No. 760935-P1.

[2] J. Davis and G.L. Kulcinski, Nucl. Fusion 16 (1976) 2.

[3] R.S. Pease, ERATOM-UKAEA Assoc. on Fusion Res., Pulsed Fusion Reactors, Int. School of Fusion Technol., Erice-Trapani, Sicily (1974).

[4] N. Ghoniem and G.L. Kulcinski, J. Nucl. Mat. 69 and 70 (1978) 816.

[5] N. Ghoniem, Ph. D. Thesis, Univ. Wisconsin, Madison (1977).

[6] N. Ghoniem and G.L. Kulcinski, Radiation Effects, to be published.

[7] C.W. Gear, Numerical Initial Value Problems in Ordinary Differential Equations (Prentice-Hall, Englewood Cliffs, NJ, 1971).

[8] N. Ghoniem and G.L. Kulcinski, Univ. Wisconsin, Fusion Design Report, UWFDM-181 (1977).

[9] R.W. Conn, G.L. Kulcinski and C.W. Maynard, to be published in Proc. 3rd Topical Meeting on Controlled Fusion Technology, Santa Fe, NM, May 9–11, 1978.

[10] R. Bullough, B.L. Eyre and R. Krishan, Proc. R. Soc., London, A-346 (1975) 81.

[11] J.M. Bunch et al., 5th Symp. on Engineering Problems of Fusion Research, Princeton Univ. (1975).

[12] F. Beranek and R.W. Conn, to be published.

[13] T.O. Hunter and G.L. Kulcinski, J. Nucl. Mat., 76 and 77 (1978) 383.

[14] T.O. Hunter and G.L. Kulcinski, Nucl. Fusion, to be published.

[15] J.A. Maniscalco, W.R. Meier and M.J. Monster, Trans. Am. Nucl. Soc. 27 (1977) 34.

[16] G.L. Kulcinski, University of Wisconsin, Fusion Design Report UWFDM-250 (1978).